http://dx.doi.org/10.21611/qirt.2012.338

QIRT 2012

11th International Conference on
Quantitative InfraRed Thermography

Use of Infrared Photography for Objective Measurement of Leg Ulcer Area in Sickle Cell Anemia Patients

by N. Malik*, C.P. Minniti**, J. Maivelett*, A. Koroulakis*, K. Delaney**, A. Buscetta**, K. Axelrod**, G.J. Kato**, and A.M. Gorbach*

* Infrared Imaging & Thermometry Unit, NIBIB, NIH, Bethesda, MD, USA, *gorbacha@mail.nih.gov*
** Sickle Cell Vascular Disease Section, Hematology Branch, NHLBI, NIH, Bethesda, MD, USA

Abstract

Measurement of skin ulcer area is essential for accurate assessment of the efficacy of different therapeutic strategies. Currently, measurement options involve subjective evaluation of ulcer borders. We quantified ulcer surface area in twelve sickle cell anemia patients by using an infrared (IR) camera and compared measurements to those obtained with standard, manual techniques that utilize visible light. IR photography is sensitive to ulcer border irregularity and capable of discerning thin epithelialization layers that are invisible, due to transparency, to the human eye or ordinary photography. The technique is non-invasive, objective, and capable of visualizing ulcers through thin dressings.

1. Introduction

Leg ulcers are encountered worldwide, and about 2% of the adult population has a history of chronic lower limb ulceration [1,2]. Sickle cell disease (SCD) is an inherited disease characterized by abnormal hemoglobin and chronic anemia with consequent end organ damage and shortened life expectancy. This disorder affects millions of people worldwide and about 100,000 individuals in North America. One of the chronic complications of sickle cell disease is recurrent leg ulcers, which have a much higher prevalence than in the rest of the population, affecting up to 20 % of SCD adults, and are responsible for significant morbidity and decline in quality of life [3,4]. Ulcers from SCD typically occur in areas of less subcutaneous fat, thin skin, and decreased blood flow--most commonly at the medial and lateral malleoli (ankles) [3].

The measurement of ulcer area is essential for assessing ulcer status and the efficacy of different therapeutic strategies. There are two basic methods of measurement: contact and non-contact with the affected skin.

Techniques that require exposure and contact with the ulcer include length and width measurements with a disposable ruler and transparency tracings. Ruler measurements have been shown to be reliable (defined as high intra- and inter- measurer consistency) [5,6,7] and capable of predicting healing [8], even though they tend to overestimate ulcer size [5,6,9,10] and are influenced by wound shape [5,11]. Transparency tracings have also been shown to have high reliability [7], but can be tedious and susceptible to subjectivity [6].

Non-contact techniques include visible light photography or computerized planimetry of digital images [5,6,11,12]. These techniques are costlier than contact techniques [5,6], however, they avoid contamination and potential damage to the wound bed [5,6]. Though these techniques have been shown to provide reliable measurements [5,11], they require that the ulcer border be subjectively distinguished from surrounding tissue based on the observer's interpretation of color or texture changes in the ulcerated area [12].

An objective and non-invasive method to measure ulcer size in real time is desirable. Assessment of leg ulcers with infrared (IR) photography has not been specifically reported in sickle cell patients. Thermography of other types of wounds, such as pressure ulcers [13], diabetic foot ulcers [14], and burn wounds [15] indicate that wound temperature is less than that of surrounding tissue. The relatively low temperature of burn wounds was attributed to evaporative cooling at the moist ulcer surface [15]. However, no attempts were made to quantify wound area using this cooling effect. When moist parts of SCD ulcers are exposed to the air they will undergo evaporative cooling, and thus be discernible by IR photography from warmer surrounding tissue. We hypothesize that, although regions covered by thin epithelialization are a potential signature of healing, they will be optically transparent to visible light photography. We predict that because these sections are much less permeable to evaporation, they will be measurably warmer than regions of exposed ulcer, and the border between the epithelial tissue and the ulcer exposed to air should be identifiable with IR photography. Further, because of heat's ability to diffuse, a temperature difference between the ulcer and its surrounding should be visible in real time even when the ulcer is covered with a thin dressing.

2. Methods

Twelve (n = 12) adult subjects with homozygous sickle cell anemia presenting with leg ulcers were studied. Patient age ranged from 22 to 59 years with a median age of 40.5 years at the time of study and included 5 male and 7 female subjects. Patients' ulcers measured between 2.51 cm^2 and 7.54 cm^2, according to visible light photography tracings, with a median size of 4.055 cm^2. All studied ulcers were located distally on the medial or lateral aspect of the

left leg. Ulcer chronicity for most patients was between 2 months and 2 years, though one patient reported chronicity of 26 years.

Prior to size measurement, all ulcers were cleaned and allowed to acclimate for at least 15 minutes. Ruler measurements for ulcer length and width were obtained using a standard measuring tape. Visible light photography was obtained using a digital camera (model EOS Rebel T2i Canon, USA) by directing the lens of the camera perpendicular to the ulcer surface from a distance of 0.25 – 0.5 m. Ulcers within visible light photos were traced manually (ENVI 4.3 software, ITT Industries, Inc., USA). The ulcer area was calculated by converting the number of pixels representing the ulcer to cm^2 using a calibration square (35.48 mm x 35.62 mm x 6.52 mm) that was placed near the ulcer for reference and easily recognized in both IR and ordinary photography images (Figure 1).

Using an IR camera (Santa Barbara FocalPlane, Lockheed Martin, USA) with a sensitivity of 0.015°C (3.0 – 5.0 µm wavelength, 16 bits), thermal images (640x512 pixels/image) were collected of each ulcer over 10-20 seconds and were taken from approximately the same distance as had been done with the visible light photography. Images were taken in patients' rooms at an average room temperature of 22°C.

To enhance ulcer boundaries on the IR image, a new image was computed for each patient using a Canny edge detector [16] algorithm (Imaging toolbox, Matlab [17]). The native IR image was first cropped to include only the wound and periwound. This prevented edge detection of the interface between the leg and the surrounding room. Next, the Canny algorithm was applied to the cropped image. The algorithm utilized the local maxima of the spatial temperature gradient between the exposed ulcer and surrounding tissue to locate ulcer edges. Unconnected boundary segments from edge detection that surrounded the ulcer were manually joined at end points. Segments that did not define the ulcer border were either excluded through thresholding or manually excluded using the visible light image for reference. The number of pixels within the calculated ulcer boundary was then used to determine ulcer size. To compare the average temperature within the ulcer boundary with the average temperature of the periwound, the periwound area was defined as the region within 1.5 cm of the ulcer border that was calculated using the Canny algorithm. This width was chosen after initial qualitative observation of a localized heat "halo" surrounding the ulcer in several patients that was approximately defined by this area. An example showing wound and periwound designations is depicted in Figure 3B.

Agreement in ulcer size between pairs of techniques (ruler technique, visible light photography, and infrared photography) was assessed through calculation of Bland-Altman plots [18].

Two nurses (from the NIH Clinical Center's Wound Ostomy and Continence Nurse Unit) identified epithelialization, granulation, necrotic tissue, and macerated skin in a zoomed visible light photograph of a patient's leg ulcer. Next, we aligned the visible and IR photographs, and corresponding regions of interest (ROIs) were marked on the IR image. Features of each ROI on the IR image, including relative temperature, were described qualitatively.

IR photography was also applied in one patient to an ulcer covered by standard dressing. Temperature of the ulcer beneath the dressing (Primapore®, #66000317) was compared with the temperature of the surrounding periwound area as well as to areas of exposed skin. The size of the dressed ulcer was also calculated by smoothing the IR image and then applying the Canny algorithm, as described above. The image-smoothing algorithm used 5 iterations of a 3 x 3 sliding window that set the value of the center pixel to the average of all pixels within the window. Sizes of the exposed wound in IR photography, exposed wound in visible light photography, and covered wound in IR photography were compared.

3. Results

Leg ulcers identified on IR images were found to be colder than surrounding areas in all patients (n = 12). An example is shown in Figure 1B. As a pilot trial, a single IR photo of the lateral malleolar area (Figure 1A) in a subject without an ulcer (n = 1) was taken for comparison and showed relative temperature uniformity.

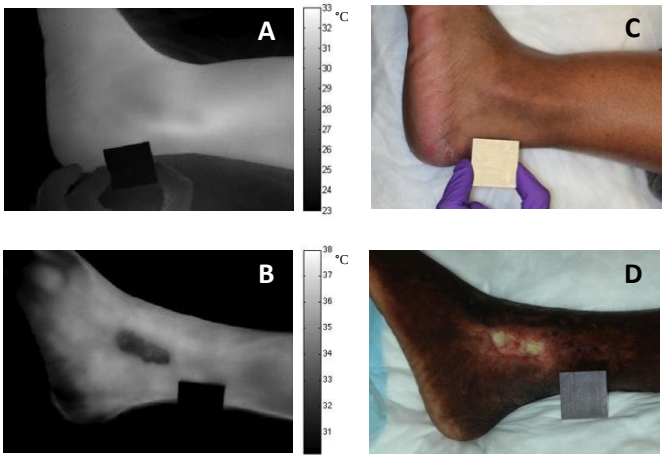

Fig. 1. *IR images of a healthy volunteer's leg (A) and an SCD patient's leg ulcer (B). Visible light images of both subjects are shown for reference (C, D). Note the same calibration square in all images.*

http://dx.doi.org/10.21611/qirt.2012.338

With acquired IR images of leg ulcers (Figure 2A) and computed spatial temperature gradient images (Figure 2B), we were able to calculate leg ulcer areas for all patients (n = 12). For comparison, leg ulcer areas were also calculated utilizing visible light images of patients' ulcers (Figure 2C). The ulcers were cooler than peripheral tissue (Figure 2A), and temperature heterogeneity was noted both within and around the ulcers.

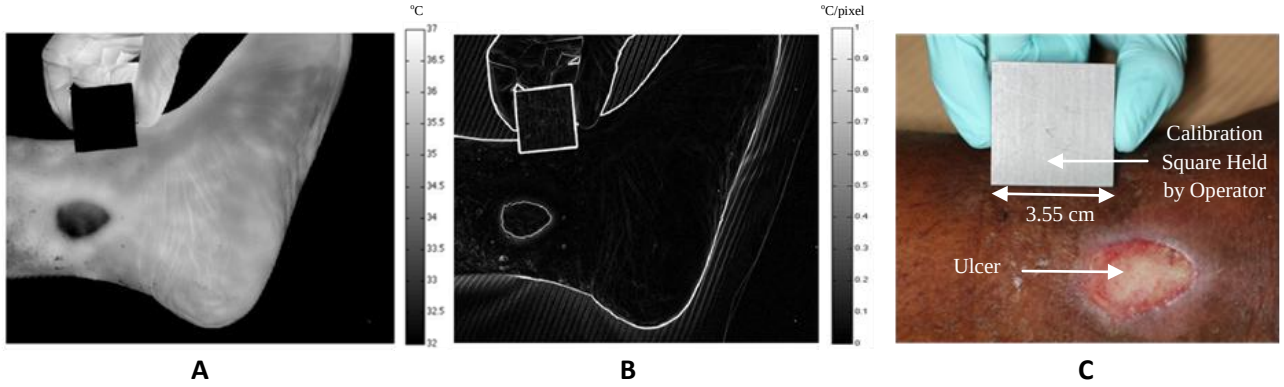

Fig. 2. *Representative SCD patient with a leg ulcer. An acquired IR image (A), calculated spatial temperature gradient image (B), and visible light image (C) are shown. The distinctive border of the ulcer in (B) is enhanced using a Canny edge detector algorithm. Note varying temperature within the ulcer and the surrounding tissue in (A). The calibration square used for size reference in visible light and IR photographs is labeled in Figure 2C and visible in 2A and 2B.*

On average, the measured ulcer temperature was 32.42 ± 1.31°C, while the defined periwound temperature was 33.97 ± 1.25°C. For all patients, ulcer temperatures were significantly less ($p < 0.0001$) than their corresponding periwound temperatures (Figure 3A). To calculate the average temperature over periwound, a ~1.5 cm wide belt-shaped area was chosen to overlay a warm "halo" around the ulcer (Figure 3B).

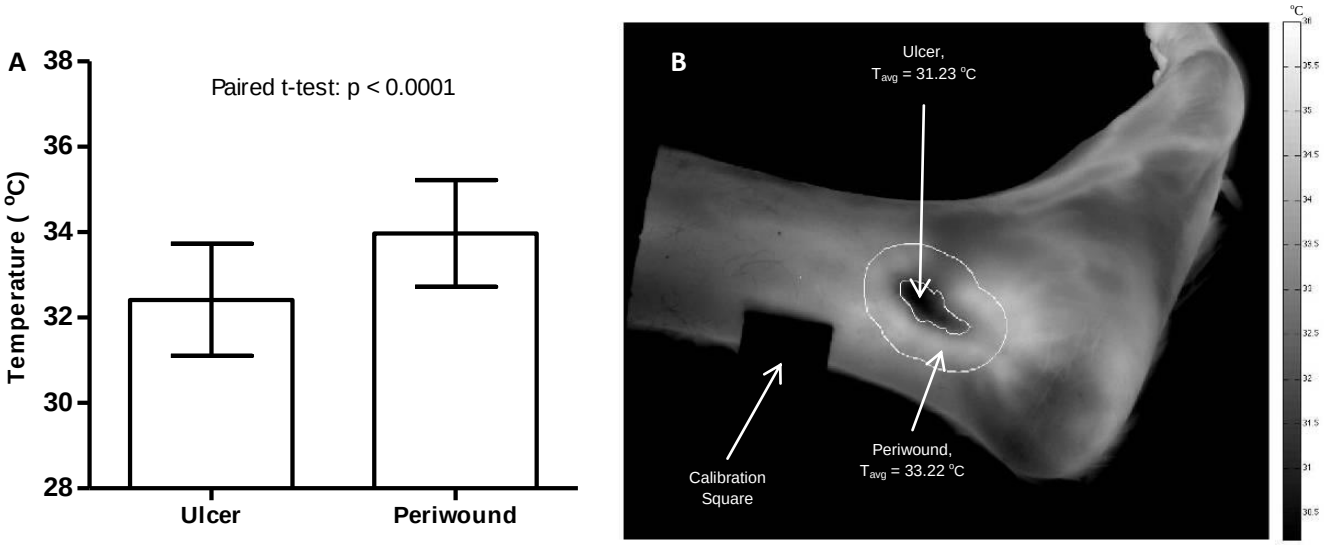

Fig. 3. *Ulcer and periwound temperatures for patient group (n = 12). (A) The average temperature of all ulcers was less than the average temperature of the corresponding periwound areas. A paired t-test was utilized to determine significance. (B) A representative ulcer with its temperature (mean over all ulcer pixels), computed ulcer and periwound borders (white lines), and periwound temperature (mean over all periwound pixels) are shown.*

A significant difference ($p < 0.05$) between measurements of ulcer areas for patients (n = 12) using a ruler, visible light photography, and IR photography was found (Figure 4).

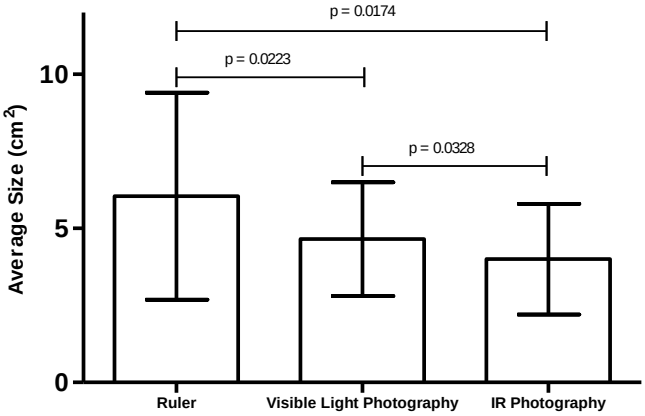

Fig. 4. *Average ulcer size measured with a ruler, visible light photography, and IR photography. The average ulcer size and standard deviation for the whole patient group are shown by modality. The p-values between each modality were calculated with paired t-tests.*

Positive slopes in linear regression of average values vs. difference were found in Bland-Altman plots between ruler and visible light photography measurements (Figure 5A) and between ruler and IR photography measurements (Figure 5B). Both slopes were significantly different from zero, with p-values of p = 0.005 and p = 0.0174, respectively. However, the slope of the linear regression line for visible light and IR photography (Figure 5C) was not significantly different from zero (p = 0.8669). Therefore, ruler measurement appears to exhibit a proportional bias in ulcer size measurement, whereas IR photography does not. Furthermore, the limits of agreement, indicated by dotted lines, showed larger ranges in Figures 5A and B than in C.

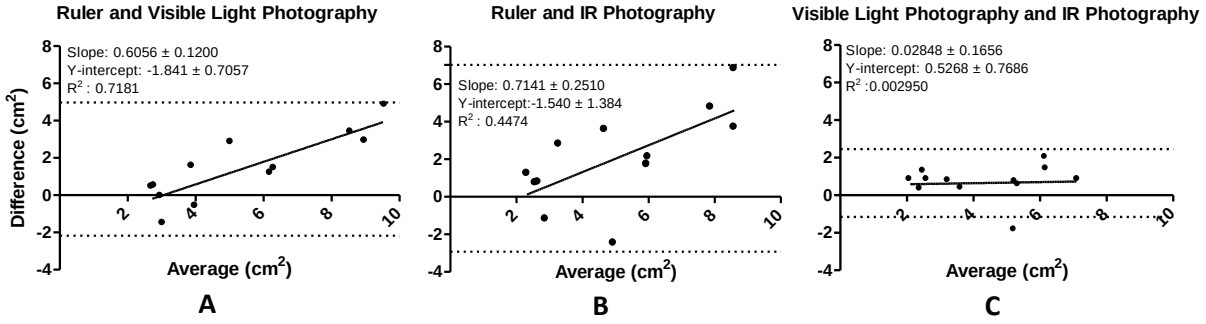

Fig. 5. *Bland-Altman plots across modalities for measurement of ulcer areas. Dotted lines indicate the limits of agreement. A linear regression was calculated for ruler and visible light photography measurements (A), for ruler and IR photography measurements (B), and for visible light and IR photography measurements (C). Note that the slopes of the regression lines in (A) and (B) are positive and significantly different from zero (p = 0.005 and p = 0.0174, respectively). The slope of the regression line in (C), however, was not significantly different from 0 (p = 0.8669).*

The calculated bias, standard deviation of bias, and 95% limits of agreement are given in Table 1 for each modality pair.

Table 1.

Modality Pair	Bias	SD of Bias	95% Limits of Agreement	
			From	To
Ruler and Visible Light Photography	1.398	1.824	-2.176	4.973
Ruler and IR Photography	2.048	2.537	-2.924	7.02
Visible Light and IR Photography	0.65	0.9229	-1.159	2.459

Three well-characterized ROIs in a zoomed visible light image of a single patient's ulcer (Figure 6A) were identified on a corresponding zoomed IR image (Figure 6B). ROI 1, characterized as granulation tissue in the visible light image due to its redness, corresponded to a region that was cooler than the remainder of the ulcer in the IR image. ROI 2, identified as a region of necrotic tissue (slough) in the visible light image due to its white/yellow appearance, corresponded to a region of median temperature within the ulcer area in the IR image. ROI 3, an area of healing tissue at

the ulcer border, was identified as epithelialization. Further, macerated skin could also be identified in ROI 3 of the visible light image due to the whiteness of its appearance. These regions, compared to the entire ulcer in the IR image, were areas of relative hotness.

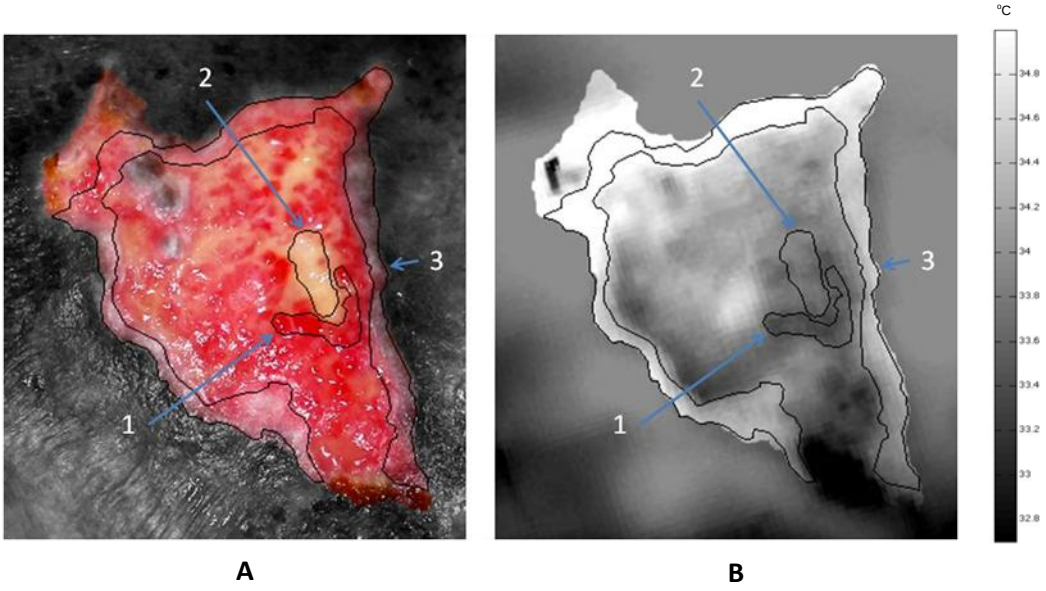

Fig. 6. *Temperature markers of ulcer granulation and epithelialization. A visible light image (A) and an IR image (B) of a leg ulcer were aligned and zoomed for a selected patient. To enhance images of the ulcer area, the periwound area was converted to grayscale in the visible image and reduced in brightness in the IR image. Three corresponding ROIs were marked in both images for qualitative comparison.*

Figure 7 shows an IR photograph of an ulcer before (A) and after (B) the application of a dressing. Note that the ulcer is cooler than the periwound prior to the application of dressing and warmer than the periwound after the application of dressing. The ulcer measured 3.79 cm^2 in the visible light photograph of the exposed wound, 3.13 cm^2 in the IR photograph of the exposed wound, and 2.04 cm^2 in the IR photograph of the dressed wound.

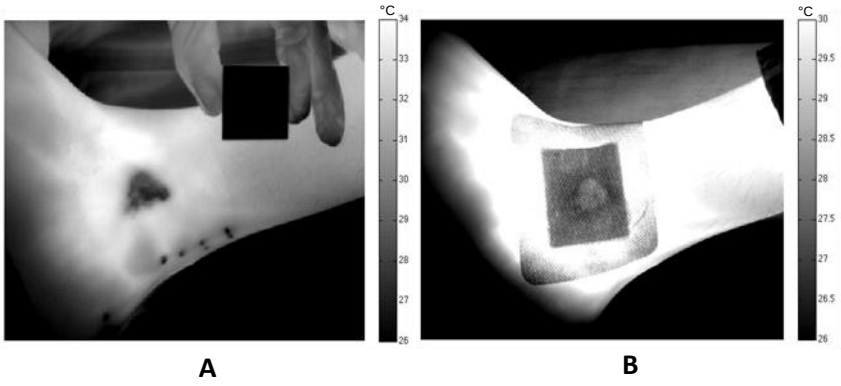

Fig. 7. *Visualization of an ulcer through a dressing. IR photographs of (A) an undressed ulcer and of (B) the same ulcer after application of a dressing (Primapore®, #66000317). Note that the ulcer was warmer than the periwound in (B).*

4. Discussion and Conclusion

Substantial temperature differences were observed between IR photographs of the left lateral malleolus of a healthy volunteer and of an SCD patient. Compared to the SCD patient's leg, the healthy volunteer's leg appeared relatively uniform in temperature (Figure 1A). The SCD patient's ulcer was clearly visible on the IR image and appeared cooler than surrounding skin (Figure 1B). These observations can be explained by the fact that the ulcer was moist and underwent evaporative cooling, consistent with previous findings [13,14,15]. Temperature, therefore, could be used as a marker for ulcer area.

An algorithm incorporating a Canny edge detector was used (Figure 2B) to determine the ulcer border on the native IR images (Figure 2A). This algorithm utilized the spatial differences in temperature between the ulcer and its periphery. The ability to determine ulcer border using temperature measurements indicates the potential of IR to quantify ulcer area objectively and automatically. This would avoid the limitations of more commonly used techniques, such as manual tracings of visible light photographs (Figure 2C), which require the ulcer border to be subjectively determined according to tissue color.

On average for the entire group of patients, as shown in Figure 3A, ulcer temperatures were 1.55°C colder than periwound temperatures ($p < 0.0001$). This difference supports the use of temperature in assessment of ulcer area.

In general, ruler measurements of leg ulcers were largest, followed by visible light photography tracings, and lastly by IR photography measurements (Figure 4). The result for ruler measurements is consistent with previous findings [5,6,9,10]. Epithelialization is transparent to visible light, and thus not visible in visible light photographs. This makes visible light images of ulcers appear larger than their "true", exposed to the air, area. Epithelialization, however, is visible by IR because it reduces evaporative cooling, thereby warming the ulcer surface. Epithelial cell recruitment in wound healing tends to begin from the wound border and progress towards the center of the ulcer [19,20], and thus ulcers appear smaller (closer to their true size) in the IR images.

The Bland-Altman plots of ruler measurements with visible light photography and IR photography measurements (Figures 5A and 5B, respectively) showed significantly positive slopes. These results indicate that the difference in size between ruler and both other measurement modalities increases for larger ulcers. The Bland-Altman plot for IR photography and visible light photography measurements (Figure 5C), however, showed a slope that is not significantly different from zero. This indicates that the difference between IR photography and visible light photography measurements is independent of ulcer size. Thus, ruler measurements inherently exhibit a proportional bias and show greater overestimation for larger ulcers, whereas IR photography does not. Note the single outlier in Figure 5C, which is below the lower limit of agreement. Eliminating this single data point (not shown) will not change the result.

Because surface temperature is dependent on blood flow and metabolic thermogenesis, we predict that the temperature may be a marker for the healing stage of an ulcer. Higher temperatures would indicate a greater degree of vascularization or greater metabolic activity, which could reveal information about the progress of wound healing. We compared temperature of a heterogeneous ulcer bed with known characteristics of ulcer pathophysiology. Epithelialization, which occurred in ROI 3 of Figure 6, appeared relatively warmer than most other regions of the ulcer on IR photography. This result is consistent with the claim that epithelialization sites block evaporative cooling and warm up via thermal conduction from the ulcer bed. Other results, however, are more counter-intuitive. ROI 1 (granulation) appears colder than other ulcer areas. Granulation is characterized by the initial formation of an extracellular matrix, immune response, and vascularization [21]. In particular, the early "granular" appearance of the wound can be described as capillary loops in the loose collagen matrix [21]. As healing progresses, small vessels may aggregate into larger vessels, and metabolic activity in the granulation tissue may change [21].

ROI 2 was intermediate in temperature, though it is co-localized with necrotic tissue (slough) that is associated with reduced blood flow. Likely, variability in wetness within the ulcer contributes to this result. We may conclude that, compared with the ulcer surrounding, relatively warm sites within the ulcer border are probably influenced by blood flow, metabolism, and bacterial content, whereas relatively cold sites may primarily be influenced by evaporative cooling due to ulcer wetness.

Imaging of the ulcer covered in dressing (Figure 7) depicted the ulcer beneath the covering. By blocking evaporative cooling with dressing, thermal conduction between the ulcer surface and the dressing can explain relatively good ulcer visibility on the IR image. Further, a "true" ulcer temperature (without evaporative cooling) can be depicted, which may provide information regarding various forms of heat accumulation (possibly including that due to microbial-related thermogenesis, neovascularization, etc.) and the likeliness of spontaneous healing [22].

Quantitatively, there is large variation in ulcer size between exposed visible light photography, exposed IR photography, and dressed ulcer IR photography measurements. This may occur because of mechanical deformation of the dressing and the dressing's porosity, permitting some heterogeneous evaporative cooling. Despite variation, there is potential for this technique to reduce the frequency of dressing removal to visualize ulcers, because the heat of ulcers is able to conduct through dressings and be visible via IR imaging. Further modification of the IR size measurement algorithm for dressed ulcers or modification of the dressing's composition may improve accuracy.

Though ulcer measurements by IR photography have the potential to be fully automated and objective, there are a few limitations to the technique. The measurements require ulcer acclimation to room temperature for at least 15 minutes in order to eliminate any external source of wetness on the periwound skin. In addition, scabs and dead skin, which lack blood perfusion, appear colder than viable skin tissue in IR imaging and may contribute artifacts to measurement. However, these areas may perhaps be eliminated or excluded through thresholding.

In summary, IR photography has several advantages for wound assessment. First, our preliminary study shows that IR photography is capable of measuring ulcer area non-invasively in real time—and it has the potential to be automated and fully objective. Second, the epithelialization layer is transparent to the human eye, but less so to IR signals. Standard measurement techniques rely on tissue color, whereas IR photography relies on greater evaporative cooling of the non-epithelialized surface. Third, intermodal differences between IR and visible light photography measurements are independent of ulcer size, whereas ruler measurements show larger intermodal differences in size for larger ulcers. Fourth, ulcer heterogeneity in IR photography may indicate signatures of healing, in particular, epithelialization and granulation. Finally, ulcers can be visualized through thin dressings using IR imaging, which could reduce the need to expose ulcers to the air for real-time wound health assessment.

5. Acknowledgements

This research was supported by the Intramural Research Program of the National Institute of Biomedical Imaging and Bioengineering, and by the Division of Intramural Research of the National Heart, Lung and Blood Institute at the National Institutes of Health. We would like to thank Dr. Henry Eden for proofreading this manuscript and for his guidance in this work. We acknowledge the expert protocol coordination by Marlene Peters-Lawrence and protocol management by Mary K. Hall.

REFERENCES

[1] Nelzen O., Bergqvist D., Lindhagen A., "The prevalence of chronic lower-limb ulceration has been underestimated: results of a validated population questionnaire". The British Journal of Surgery, vol. 83, pp. 255-258, 1996.
[2] Graham I.D., Harrison M.B., Nelson E.A., Lorimer K., Fisher A., "Prevalence of lower-limb ulceration: a systematic review of prevalence studies". Advances in Skin & Wound Care, vol. 16, pp. 305-316, 2003.
[3] Minniti C.P., Eckman J., Sebastiani P., Steinberg M.H., Ballas S.K., "Leg ulcers in sickle cell disease". American Journal of Hematology, vol. 85, pp. 831-833, 2010.
[4] Koshy M., Entsuah R., Koranda A., Kraus P., Johnson R., Bellvue R., Flournoy-Gill Z., Levyet P., "Leg ulcers in patients with sickle cell disease". Blood, vol. 74, pp. 1403-1408, 1989.
[5] Thawer H.A., Houghton P.E., Woodbury M.G., Keast D., Campbell K., "A comparison of computer-assisted and manual wound size measurement". Ostomy/Wound Management, vol. 48, pp. 46-53, 2002.
[6] Brown D., "Comparing different ulcer measurement techniques: a pilot study". Primary Intention: The Australian Journal of Wound Management, vol. 11, pp. 125-134, 2003.
[7] Majeske C., "Reliability of wound surface area measurements". Physical Therapy, vol. 72, pp. 138-141, 1992.
[8] Kantor J., Margolis D.J., "Efficacy and prognostic value of simple wound measurements". Archives of Dermatology, vol.134, pp. 1571-1574, 1998.
[9] Langemo D., Anderson J., Hanson D., Hunter S., Thompson P., "Measuring wound length, width, and area: which technique?" Advances in Skin & Wound Care, vol. 21, pp. 42-45, 2008.
[10] Rogers L.C., Bevilacqua N.J., Armstrong D.G., Andros G., "Digital planimetry results in more accurate wound measurements: a comparison to standard ruler measurements". Journal of Diabetes Science and Technology, vol. 4, pp. 799-802, 2010.
[11] Mayrovitz H.N., Soontupe L.B., "Wound areas by computerized planimetry of digital images: accuracy and reliability". Advances in Skin & Wound Care, vol. 22, pp. 222-229, 2009.
[12] Haghpanah S., Bogie K., Wang X., Banks P.G., Ho C.H., "Reliability of electronic versus manual wound measurement techniques". Archives of Physical Medicine and Rehabilitation, vol. 87, pp. 1396-1402, 2006.
[13] Nakagami G., Sanada H., Iizaka S., Kadono T., Higashino T., Koyanagi H., Haga N., "Predicting delayed pressure ulcer healing using thermography: a prospective cohort study". Journal of Wound Care, vol. 19, pp. 465-466, 468, 470, 2010.
[14] Bharara M., Schoess J., Armstrong D.G., "Coming events cast their shadows before: detecting inflammation in the acute diabetic foot and the foot in remission". Diabetes/Metabolism Research and Reviews, vol. 28, suppl. S1, pp. 15-20, 2012.
[15] Newman P., Pollock M., Reid W.H., James W.B., "A practical technique for the thermographic estimation of burn depth: A preliminary report". Burns: Journal of the International Society for Burn Injuries, vol. 8, pp. 59-63, 1981.
[16] Canny J. A computational approach to edge detection. IEEE Transactions on Pattern Analysis and Machine Intelligence, vol. 8, pp. 679-698, 1986.
[17] MATLAB. In. 7.10.0.499. ed: The MathWorks Inc.; 2010.
[18] Bland J.M., Altman D.G., "Statistical methods for assessing agreement between two methods of clinical measurement". Lancet, vol. 1, pp. 307-310, 1986.
[19] Schultz G.S., Sibbald G.R., Falanga V., Ayello E.A., Dowsett C., Harding K., Romanelli M., Stacey M.C., Teot L., Vanscheidt W., "Wound bed preparation: a systematic approach to wound management". Wound Repair and Regeneration, vol.11, pp.1-28, 2003.
[20] Repesh L.A., Fitzgerald T.J., Furcht L.T., "Fibronectin involvement in granulation tissue and wound healing in rabbits". The Journal of Histochemistry and Cytochemistry, vol. 30, pp. 351-358, 1982.
[21] Schultz G.S., Ladwig G., Wysocki A., "Extracellular matrix: review of its roles in acute and chronic wounds". World Wide Wounds, Available at: http://www.worldwidewounds.com/2005/august/Schultz/Extrace-Matric-Acute-Chronic-Wounds.html, 2005.
[22] Cole R.P., Shakespeare P.G., Chissell H.G., Jones S.G., "Thermographic assessment of burns using a nonpermeable membrane as wound covering". Journal of the International Society for Burn Injuries, vol. 17, pp. 117-122, 1991.